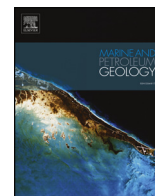




ELSEVIER

Contents lists available at ScienceDirect

Marine and Petroleum Geology

journal homepage: www.elsevier.com/locate/marpetgeo

Research paper

First documentation of seismic stratigraphy and depositional signatures of Zhongsha atoll (Macclesfield Bank), South China Sea

Xiaoxia Huang^{a,b,*}, Christian Betzler^c, Shiguo Wu^a, Anne Bernhardt^b, Graeme Eagles^d, Xiaohui Han^e, Martin Hovland^f

^a Laboratory of Marine Geophysics and Georesources, Institute of Deep-sea Science and Engineering, CAS, China

^b Institute of Geological Sciences, Freie Universität Berlin, Berlin, 12249, Germany

^c University of Hamburg, Center for Earth System Research and Sustainability, Institute of Biogeochemistry and Marine Chemistry, Hamburg, Germany

^d Alfred-Wegener-Institut Helmholtz-Zentrum für Polar- und Meeresforschung, Germany

^e Marine Geological Survey Institute of Hainan Province, Haikou, China

^f Tech Team Solutions, Stavanger, 4036, Norway

ARTICLE INFO

Keywords:

Zhongsha atoll
South China Sea
Reefs
Seismic reflection
Lagoon
Carbonates

ABSTRACT

Carbonate platforms form informative archives for paleoclimates and their internal structures can also hold crucial information about the tectonic history and carbonate evolution of the ocean basins. The Zhongsha atoll (Macclesfield Bank) forms the largest atoll system in the South China Sea with a surface area of 23500 km². However, the internal structure and evolution of this atoll system is completely unknown. 2D multichannel seismic reflection data were acquired in 2017 over the Zhongsha atoll in the South China Sea to unravel the stratigraphy, geomorphology, depositional processes, and seismic facies of one of the world's largest atoll for the first time. This Neogene carbonate platform comprises more than 1 km thick carbonate sequence and overlies a metamorphic basement. The southeastern part of the atoll comprises a fault-controlled graben system, which was formed during the Cenozoic rifting stage of the South China Sea. Most of the faults trend NE-SW and E-W and terminate at or slightly above the top of Middle Miocene strata. Atolls and abundant organic reefs initiated on the positive relief and closely mimicked the underlying topography during the Early Miocene. Shallow-water carbonates continued growing through Middle Miocene to present times. Regional uplift led to subaerial exposure, termination of platform growth and karstification during the Miocene. We also reveal a number of fluid-flow features such as vertical sub-bottom venting features (chimneys and pipes), chaotic reflection zones, which provide the first evidence of active fluid venting in the area of Zhongsha atoll. The Neogene sedimentation history of Zhongsha atoll further provide an important paleoenvironmental context for future scientific drilling to better constrain the evolution of Asia Monsoon.

1. Introduction

Atolls are ring-shaped reef complexes. The most extensive groups of atolls occur in the Pacific Ocean but there are also numerous atolls in the central Indian Ocean and the South China Sea (SCS) (Burger and Gochfeld, 2000; Betzler et al., 2009, 2013; Jorjy and Bièvre, 2011). The SCS is a marginal sea of the Pacific Ocean, affected by the South Asian Monsoon belt (Ha et al., 2018), climatically in a tropical and subtropical area (23 °N–4 °N) (Fig. 1). Here, atolls and reefs developed extensively in Miocene times as carbonate platforms built up during regional transgressions onto relict positive reliefs (Wilson, 2008; Fyhn et al., 2013). Ever since then, the platform's evolution has been determined by the interplay of tectonic subsidence, sea-level changes,

ocean currents, and regional environmental change (Martin et al., 1996; Schlager, 1999; Lukasik et al., 2008; Wu et al., 2014; Wang et al., 2014; Shao et al., 2017). In the northern SCS, carbonate platforms started to develop along the shelf edge in the Late Oligocene and achieved a maximum expansion during the Early Miocene (Wu et al., 2016). Most of these northern platforms were subsequently drowned during the early Middle Miocene, in response to the local subsidence along the northern margin and a global sea level rise (Zampetti et al., 2004, 2005; Fyhn et al., 2009; Fyhn et al., 2013).

The Zhongsha atoll (Fig. 1) is a ring of shoals arranged along the outer rim of a drowned atoll structure. Zhongsha atoll has not been drilled so far. It is covered by recently acquired four wide-angle seismic reflection profiles, which together with the multichannel seismic

* Corresponding author. Laboratory of Marine Geophysics and Georesources, Institute of Deep-sea Science and Engineering, CAS, China.
E-mail address: huangxx@idsse.ac.cn (X. Huang).

<https://doi.org/10.1016/j.marpetgeo.2020.104349>

Received 17 January 2020; Received in revised form 10 March 2020; Accepted 15 March 2020

Available online 20 March 2020

0264-8172/ © 2020 Institute of Deep-Sea Science and Engineering, Chinese Academy of Sciences. Published by Elsevier Ltd. This is an open access article under the CC BY-NC-ND license (<http://creativecommons.org/licenses/by-nc-nd/4.0/>).

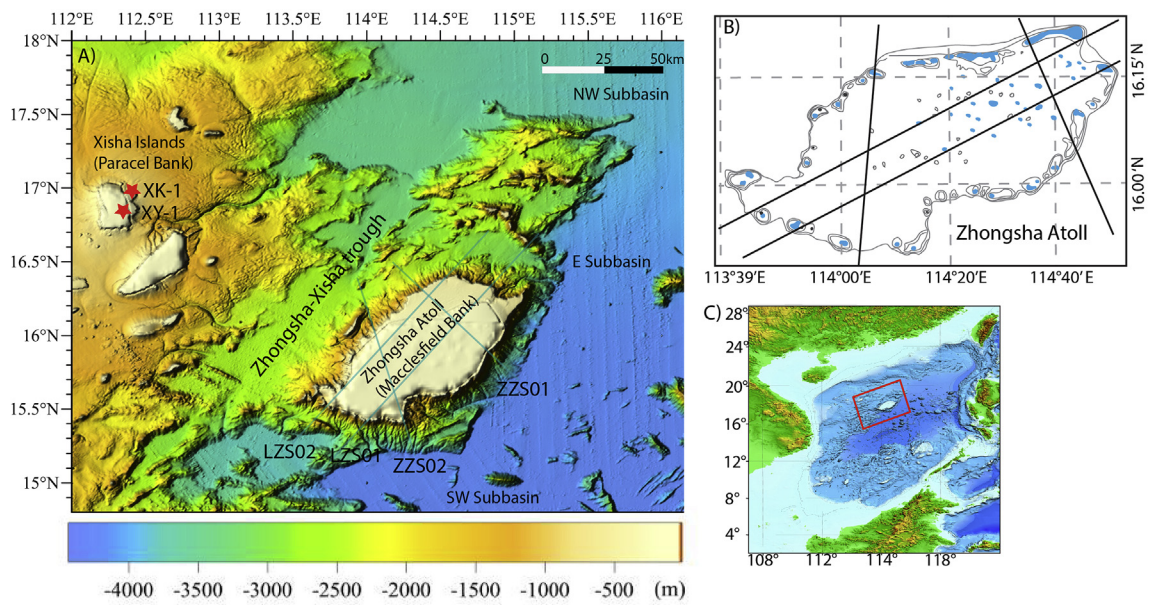


Fig. 1. Location and bathymetry of Zhongsha and Xisha, and wells XY-1 and XK-1 on Xisha, used to constrain the age of the Zhongsha seismic sequence. Light blue lines indicate the locations of seismic lines used in this study. Note that the Zhongsha atoll shows a relative flat surface because multibeam bathymetric data are not available for the interior of Zhongsha atoll. (For interpretation of the references to colour in this figure legend, the reader is referred to the Web version of this article.)

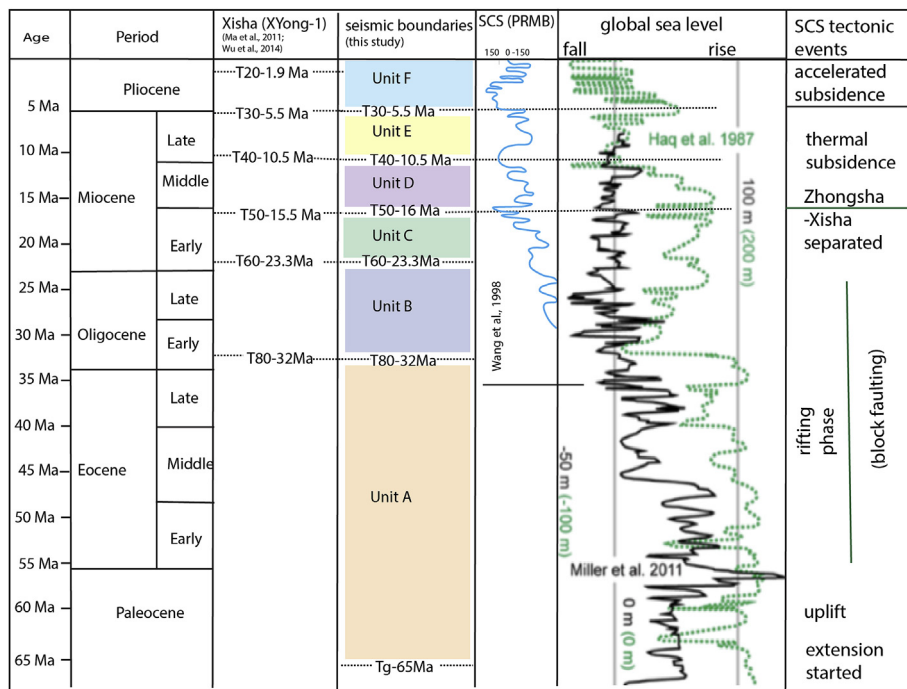


Fig. 2. Schematic seismic stratigraphic column of the Xisha-Zhongsha, based on drilling results from wells XY-1 and XK-1, and its correlations to regional SCS and global relative sea level changes (Haq et al., 1987; Miller et al., 2011; Ma et al., 2011; Wu et al., 2014; Wang et al., 2015) and regional SCS tectonic episodes.

reflection data from Xisha island, reveal that both are located on rifted blocks that appear to have been separated from the South China margin since the Early Miocene (Taylor and Hayes, 1980; Briais et al., 1993; Qiu and Wang, 2001; Qiu et al., 2004; Franke et al., 2014; Barckhausen et al., 2014). We use observations from wells XY-1 and XK-1 on Xiyong and Xisha islands to propose a stratigraphy model and a depositional history of the Zhongsha carbonate atoll (Fig. 2). Preliminary results on the lithostratigraphy and geochemistry of XK-1 and XY-1 have recently been reported in several papers (Li et al., 2006; Wang et al., 2015; Xiu et al., 2015; Shao et al., 2017).

In this study, we aim to generate a first overview of this unknown platform, which forms the largest single atoll system in the SCS with a surface area of 23500 km², and its interactions with climate, tectonics and other environmental factors. Using newly-acquired seismic-reflection data and multibeam bathymetric data, we assess and interpret some of the sub-bottom features to reveal unique information about the stratigraphy, geomorphology, depositional processes, and seismic facies of this region for the first time.

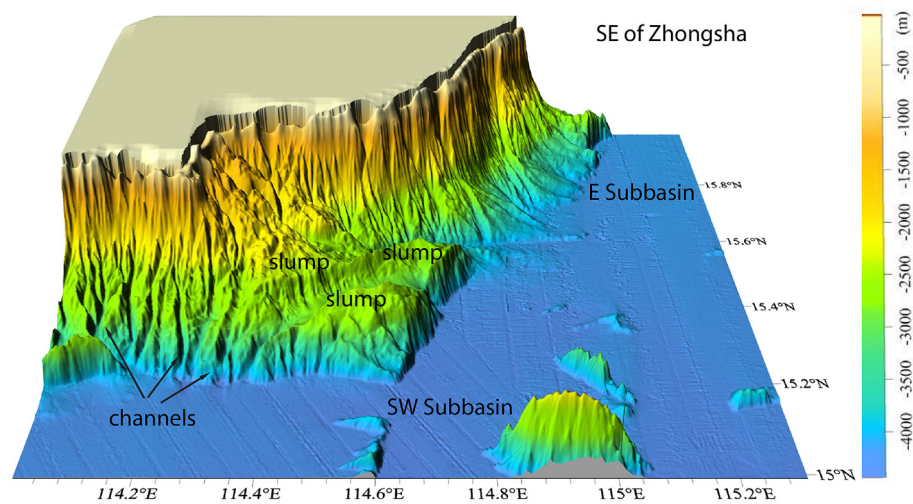


Fig. 3. The southern and eastern slopes of Zhongsha are steep, with angles of up to 90°, and are dominated by channels and by slump deposits.

2. Geological background

Zhongsha atoll (also known as Macclesfield Bank) is one of the world's largest elongated drowned atoll. The entire Zhongsha atoll covers an area of about 23500 km², its length exceeds 150 km southwest-northeast, and its maximum width exceeds 75 km. It is located between 15.4 and 16.25 °N, 113.6–115 °E in the SCS. The SCS is a product of rifting and seafloor spreading that took place between the Late Cretaceous and Early Oligocene. The Zhongsha and Xisha islands (Fig. 1) are interpreted as rigid continental blocks that rifted off the South China Block during this period, although ongoing seismicity suggests that their bounding faults are still active or were recently reactivated (Yan et al., 2014). Previous studies have concluded that continental crust underlies the Zhongsha atoll, based on seismic, gravimetric, and magnetic data and the geological similarity to the adjacent northern continental margin of the SCS (Taylor and Hayes, 1980, 1983; Briais et al., 1993). By the Early to Middle Miocene, faults bounding the Zhongsha-Xisha block on the northern margin of the southwestern sub-basin of the SCS had ceased to accommodate crustal extension. The block began to subside due to post-rift cooling and thickening of the lithosphere (Sun et al., 2009; Franke et al., 2014; Gao et al., 2016). The crustal thickness of Reed Bank and Zhongsha, once parts of the same continental block, lie in the region of 20–25 km (Nissen et al., 1995; Huang et al., 2019).

The precise nature and composition of the acoustic basement of Zhongsha atoll is still unclear. Well data from XY-1 suggests that the Zhongsha atoll and Xisha island consist of Precambrian metamorphic basement covered by more than 0.5 km of Neogene carbonate (Zhu et al., 2016; Shao et al., 2017). The northern SCS region experienced continued subsidence since Late Neogene and temperature, salinity, and water depth conditions suitable for the extensive development of coral reef carbonate strata were established (Zhang et al., 2018).

3. Data and methods

Multichannel seismic-reflection data were acquired during August and September 2017. This is the first seismic experiment across the Zhongsha atoll in the SCS. The streamer was 600 m long with 6.25 m channel separation. The source distance is 12.5 m, so the seismic system has a 90 m migration distance. Data processing was accomplished using the Omega processing platform. The original seismic data are interpreted Petrel E&P software platform [(*) = Mark of Schlumberger]. All the vertical scales for seismic profiles shown in the study are two-way travel time. Bathymetric data were collected by the Guangzhou Marine Geological Survey (GMGS) and used to image the slopes around the

atolls. The bathymetric map in Fig. 1 was made by combining the multibeam depth soundings with the predicted bathymetry from satellite data. Multibeam bathymetric data are missing from the interior of Zhongsha atoll.

4. Results

4.1. Margin structure and morphology

Zhongsha atoll is a ring-shaped drowned atoll which developed directly over the Zhongsha block and lies about 200 km southeast of Xisha (Paracel) platform. The multibeam bathymetric data record a complex system of submerged platforms with a shallowest measured water depth of 10–20 m. The platform's long edges trend NE-SW and vary in sinuosity. The submarine topography of the Zhongsha region is characterized by different morphologies, including large atoll systems, coral reefs, and canyons (Fig. 1). An elongated extension of shoals and reefs projects from the northeast corner of Zhongsha atoll (Fig. 1).

The western outer slope of Zhongsha atoll is bounded by the Zhongsha-Xisha trough, where the seafloor reaches to depths of about 2500 m. The east and south facing slopes reach down to the abyssal plain of the SCS in about 4000 m water depth, and are extremely steep, in places vertical (Fig. 3). The eastern slope is located in water depths of 500–4200 m and is steep, with angles up to 90° (Fig. 1). The average angle of the east slope is about 11°, but in its upper reaches it steepens abruptly to 30°. Numerous submarine canyons, gullies, and slumps are dominated on the north, east and south slopes (Figs. 1 and 3).

4.2. Seismic framework

Due to the lack of wells on the Zhongsha atoll, the carbonate sequences in the seismic profiles and the interpreted depositional history are referenced to observations in wells XY-1 and XK-1 from Xisha platform (Figs. 1 and 2). Seven key horizons, including the seafloor (SB, T30, T40, T50, T60, T80, and Tg) are interpreted via jump correlation and six intervals (seismic units A-F) are recognized within the study section (Fig. 2). A seismic unit is defined as a mappable interval of associated characteristic seismic reflectivity patterns (referred to as seismic facies (SF), Table 1) bounded by marker reflectors. The marker reflections coincide with distinct changes at the boundaries and likely caused by lithological and/or structural contrasts.

4.2.1. Unit A (early rift): late paleocene to Early Oligocene

Unit A fills half grabens dissecting the top of the basement, reaching thicknesses of as much as 100 ms (TWT: two-way travel time

Table 1
Seismic facies description and interpretation.

| seismic facies | reflection characteristics | Interpretation | seismic facies | reflection characteristics | Interpretation |
|----------------|---|------------------------------|----------------|--|-------------------------------------|
| SF1 | mound shape, convex-up sub-horizontal parallel reflections, continues, high amplitude | carbonate platform | SF6 | positive topography relief, continuously accumulating, layered, and generally with a chaotic weak reflection | reef rim |
| SF2 | continuous to semi-continuous, low to moderate amplitude | lagoon | SF7 | spiky strong reflectors, partly highly attenuated, and/or scattered. internal reflection are rather chaotic | pinnacle reef |
| SF3 | downlap of lower reflection terminations, sigmoidal clinoforms moderate to high amplitude | carbonate progradation Slope | SF8 | mounded external shape, internal reflectors attenuated but visible, either subparallel to seabottom or oblique | patch reef |
| SF4 | steep margin, backstepping | Platform margin, shrinking | SF9 | chaotic reflection zones or vertical discontinuous zones inside of the pipes | fluid flow seismic pipes |
| SF5 | karst facies with high amplitude, broken reflections | karstification | SF10 | vertical to subvertical columnar zones of disturbed seismic reflections (velocity pullup) | hydrothermal water, seismic chimney |

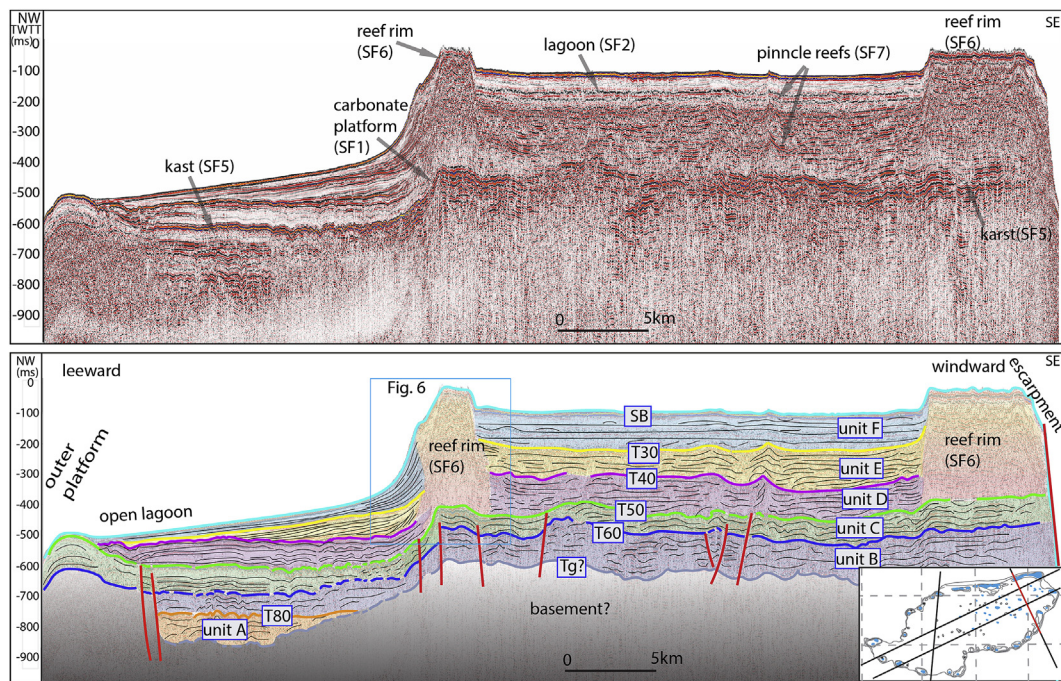


Fig. 4. NW-trending seismic profile over the eastern end of Zhongsha atoll. Seismic facies associations separated by six regional surfaces define 6 seismic units (A–F), interpreted tentatively on the basis of long distance well-ties. Faults (red lines) are observed cutting units A, B, C and terminating mostly below reflector T50. The blue dots represent the reefs. (For interpretation of the references to colour in this figure legend, the reader is referred to the Web version of this article.)

thickness), and is mainly observed in a rifted basin situated in the southeast Zhongsha atoll (Fig. 4). Reflector T80, at the top surface of Unit A, is only observed in the rifted basins and grabens. The basal reflector, Tg, represents the top of the basement with an approximate age of 65 Ma. Data quality is too poor over the Zhongsha atoll to support clear and consistent interpretations of Tg. The top of the

basement is discontinuous and cut by numerous normal faults, with a dominant SW-NE trend. Unit A is characterized by chaotic internal reflectivity with low to medium amplitudes. A general age of Late Paleocene to Early Oligocene is proposed for this package based on the comparison with the succession known from the Xisha platform (Wu et al., 2014).

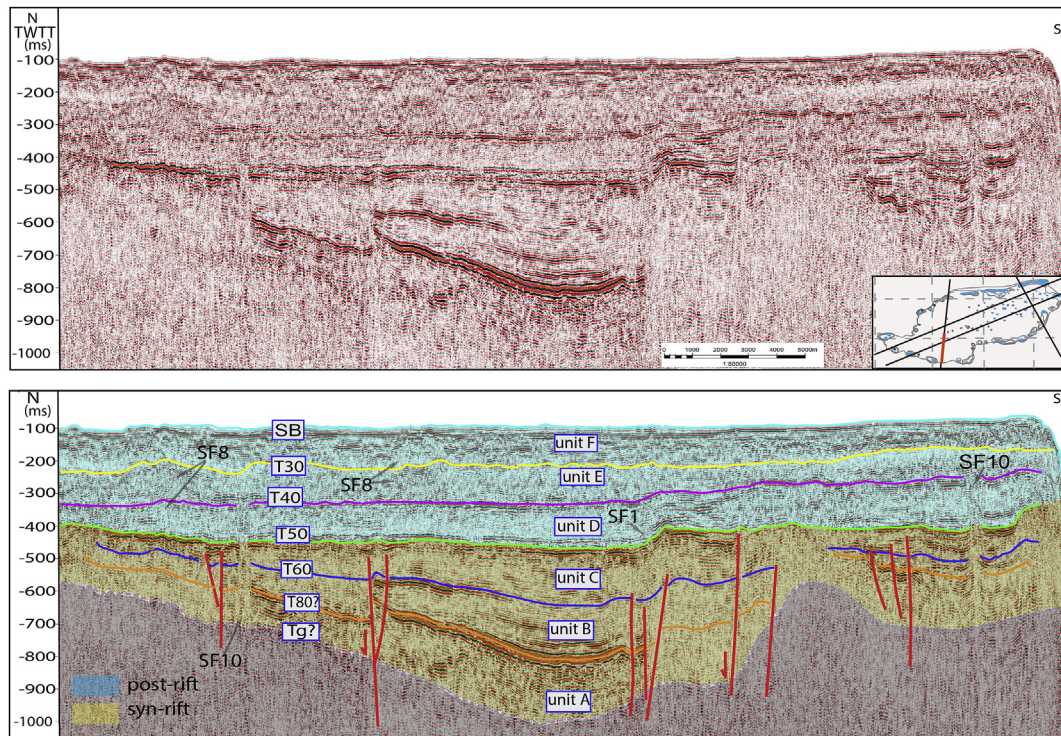


Fig. 5. A rift basin is observed at the southwest margin of Zhongsha atoll. The Reflector T50 marks the boundary between syn-rift and post-rift sequences.

4.2.2. Unit B: (Syn-rift) Early Oligocene to Early Miocene

Unit B is bounded at its base by T80 in the rift basins, where it is observed conformably overlying Unit A, and by Tg elsewhere where it overlies the basement. Its upper boundary is at T60. The maximum thickness of Unit B is about 80–100 ms (TWTT). It terminates to the east of Zhongsha atoll. The upper part of the unit shows medium to transparent reflectivity basin-fill forming onlap patterns in grabens created by the movements of the E-W and SW-NE trending faults (Fig. 5). Unit B is strongly rotated and shows large horizontal variability. Strong parallel reflectors and the syn-rift timing suggest it consists of siliciclastic deposits. The deposition of this unit is mainly controlled by E-W, SW-NE faults during rifting processes, and a general range age of Early Oligocene to Early Miocene is proposed.

4.2.3. Unit C (transition): Early Miocene

Seismic Unit C, bounded between the reflectors T60 and T50, is characterized by subparallel to parallel reflectors of low to medium amplitude and low-amplitude hummocky reflections that are cut or deformed by faults (Figs. 4 and 5). The maximum thickness of this unit is up to 80 ms (TWTT), around 160 m. Abundant mounded features indicate the first occurrences of reefs and discrete carbonate banks. Externally, the platform (characterized by SF1; Table 1) shows a convex-up morphology. Internally, SF1 is dominated by sub-horizontal, parallel reflections with high amplitudes. In the seismic profiles, chaotic reflectivity and rugged topography are observed (SF5, Table 1), indicating that the unit experienced post-depositional karstification. Unit C terminates at reflector T50, which can be traced throughout Zhongsha atoll (Figs. 4 and 5). The upper surface of the platform in Unit C is slightly tilted and recognizable by its rough fault-related topography, indicating ongoing fault activity (Figs. 4 and 5). According to the Xisha platform wells, reflector T50 dates from the Middle Miocene (15.5 Ma). We suggest that unit C is a transitional unit, which marks the shift from syn- to post-rifting in the study region.

4.2.4. Unit D (post-rift): Middle Miocene to Late Miocene

Seismic Unit D lies between reflectors T50 and T40. This unit varies

in thickness within the range of 50–150 ms (TWTT). Reflection packages range from horizontal and continuous to mounded and discontinuous, with distinct reflectivity changes and seismic stacking patterns. Isolated mounds and cones in a wide range of sizes and with internal chaotic reflection patterns and onlapping overlying reflectors are common in this unit (Figs. 4 and 5). The mounded reef rim seismic facies (SF6) is first encountered in Unit D above reflector T50. Its width is nearly 7 km and its height exceeds 100 ms TWTT. Lagoonal deposits, interpreted on the basis of continuous to semi-continuous reflectors with low to moderate amplitude, appear along with the initiation of the reef rim deposit. Reflector T40 is a widely recognizable relatively high amplitude reflector that is assigned to the Upper Miocene strata, around 10.5 Ma (Figs. 2 and 4).

4.2.5. Unit E: late Miocene

Unit E, bounded by reflectors T40 and T30, comprises late Miocene strata. The maximum thickness of this unit is about 100 ms (TWTT). Several patches and pinnacle reefs (SF7, SF8, Table 1) are interpreted to occur in the lagoon. Seismically, they are present as mounded or spiky structures with hummocky to contorted high-amplitude reflections. Progradational patterns locally vary in shape and extent but often appear as flat-topped sigmoids lapping down on to the top of Unit D (Fig. 6; SF3, Table 1). Mounds are more isolated within unit E. Karst (SF5, Table 1) features occur continuously throughout Unit E (Fig. 4).

4.2.6. Unit F: pliocene to present

Unit F is bounded by reflector T30 and the seafloor. Its maximum thickness is about 150 ms (TWTT) (Figs. 4 and 5). Two different sets of reflection patterns are identified in this unit. One is characterized by sub-parallel to parallel reflections with low to medium amplitude, interpreted as representing lagoonal deposits (SF2, Table 1). The other pattern appears within mound structures with low-amplitude chaotic to transparent reflectivity, interpretable as reefs (SF7, SF8, Table 1).

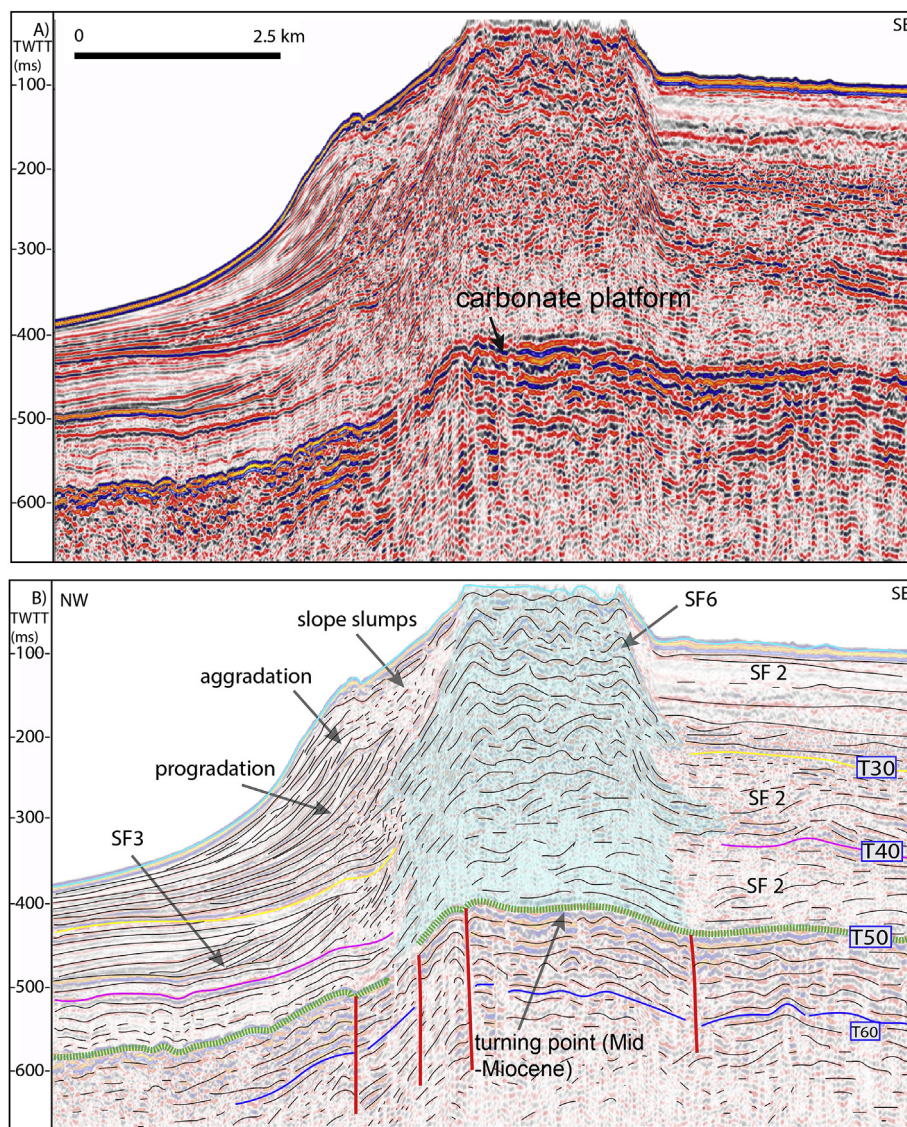


Fig. 6. Seismic expression of the reef rim with uninterpreted seismic line (A) and interpreted seismic line (B). Seismic reflection patterns changed significantly after the Middle Miocene.

4.3. Carbonate platform, reef rims, pinnacle reefs, and lagoons

4.3.1. Early to Middle Miocene carbonate platform

The seismic characteristics of the Early to Middle Miocene carbonate platform and reefs (unit C) differ from those of the surrounding strata (Fig. 4). In the study region, the Early to Middle Miocene carbonate platform is characterized by a broad tilted top surface and steep margins generated by normal faults. The platform is less than a few km wide and up to 50–100 ms thick. Its internal structure varies from high-amplitude, continuous, parallel reflections to discontinuous, mounded reflections. The top of the middle Miocene carbonate platform corresponds to the pronounced regional unconformity T50, which shows convex-up morphology. T50 is overlain by younger deposits, marking a significant hiatus which, coupled with a number of collapse structures and depressions, suggests a late Early Miocene period of platform exposure and karstification.

4.3.2. Reef rims

Atolls are characterized by well-developed reefal margins and an interior lagoon. Discontinuous marginal reefs surrounded a lagoon with water depth of up to 50–70 m. The middle Miocene was a major period of atoll development in the SCS, as can be interpreted from the internal

and external geometries of seismic reflector packages, their relationships to their neighbors, and the nature of reflector terminations. A reef rim enclosing the lagoon is recognized on the basis of its positive relief, high-amplitude, parallel, continuous reflections at the top, and its low-amplitude internal reflectivity oriented parallel to the top of basement, which suggests continuous aggradation. The width of the reef rim varies from 3 to 6 km (Figs. 4 and 6). The reef rim continued to grow from the Middle Miocene (unit D) up to the Present (unit E and F) locally and reaches a height of more than 0.5 km and is mainly developed above the Lower Miocene carbonate platform. The base of the Mid Miocene atoll is bounded by high-amplitude continuous reflections, indicating a strong impedance contrast (Fig. 6).

The clinoform facies (SF3, Fig. 6) occurs primarily at the reef rim's flank and adjacent to lagoons. The facies are identifiable on the basis of a series of distinct, subparallel, shingled clinoforms (Fig. 6). The identification of onlap termination on the shelf margin reefs is complicated by interfingering of strata from the carbonate reefs and their surroundings. The detailed stratigraphy of the clinoform indicates progradation and is particularly well developed along the northwest margin of the reef rim (Fig. 6). The lack of well control where the seismic facies are observed prevents an assessment of the exact lithologies present.

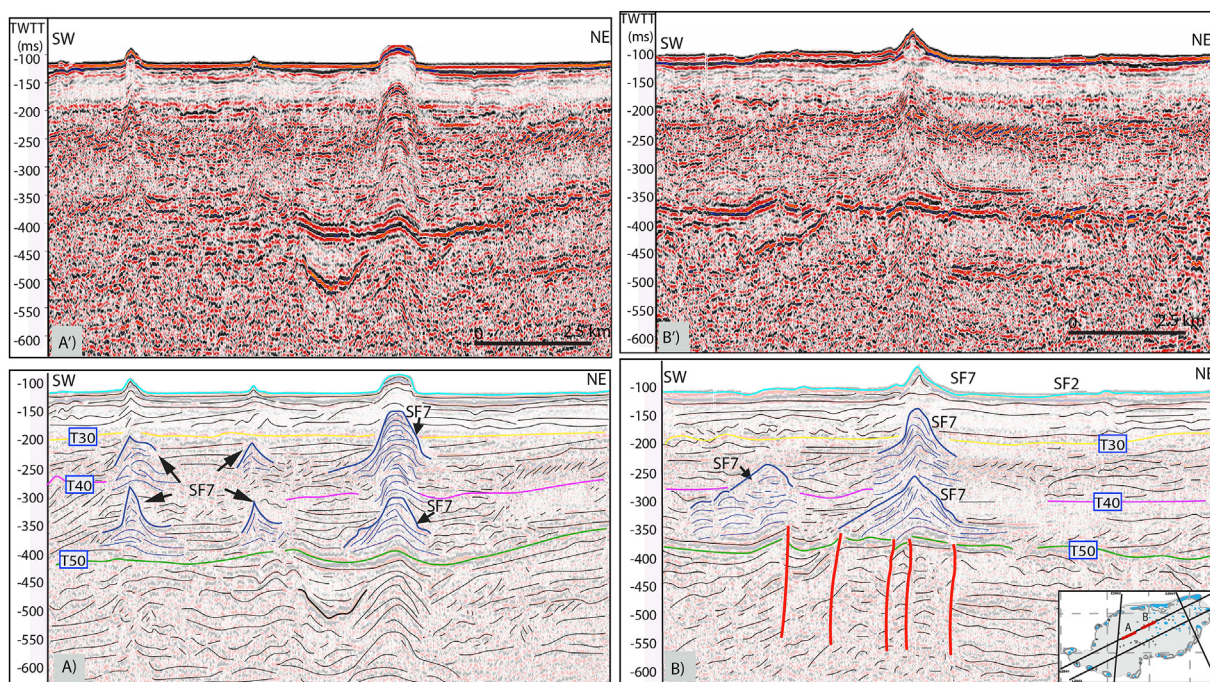


Fig. 7. Seismic expressions of pinnacle and patch reefs in the lagoon on A and B. Most of the reefs were developed between key horizons of T50 and T30.

4.3.3. Lagoons and reefs

Lagoons are major components of atoll systems and are sites of gradual infilling by carbonate sediments produced within them and at the adjacent more productive reef rim. The general depth of the lagoon floor in east Zhongsha atoll is about 50–80 m. Lagoon-filling processes produce distinct seismic facies characterized by chaotic to subparallel reflections in lensoid packages adjacent to carbonate mound structures (Figs. 4, 7 and 8). These packages onlap the mound complexes and downlap onto the underlying carbonate bank, often showing internal stratification. Seismic imaging in the lagoons was complicated because of the irregular seafloor topography caused by shallow reefs.

Over time, reef mounds became confined and stacked to form a 300 m thick reef complex (Fig. 8). The mounded discontinuous facies are identified by a series of convex-upward or mound shapes (SF7, SF8, Table 1). Typically, the flanks of a mound structure are developed in a stratigraphically lower reflection package while the crest is contained in younger packages. Within the mounds, discontinuous and individual internal reflector packages show onlapping and downlapping geometries. Mounds are separated from one another by packages of continuous to discontinuous horizontal, parallel reflectors. Mounds frequently occur in the lagoons. Based on their stratigraphic interval and seismic signatures, the mounds and ridges are interpreted as reefs. The

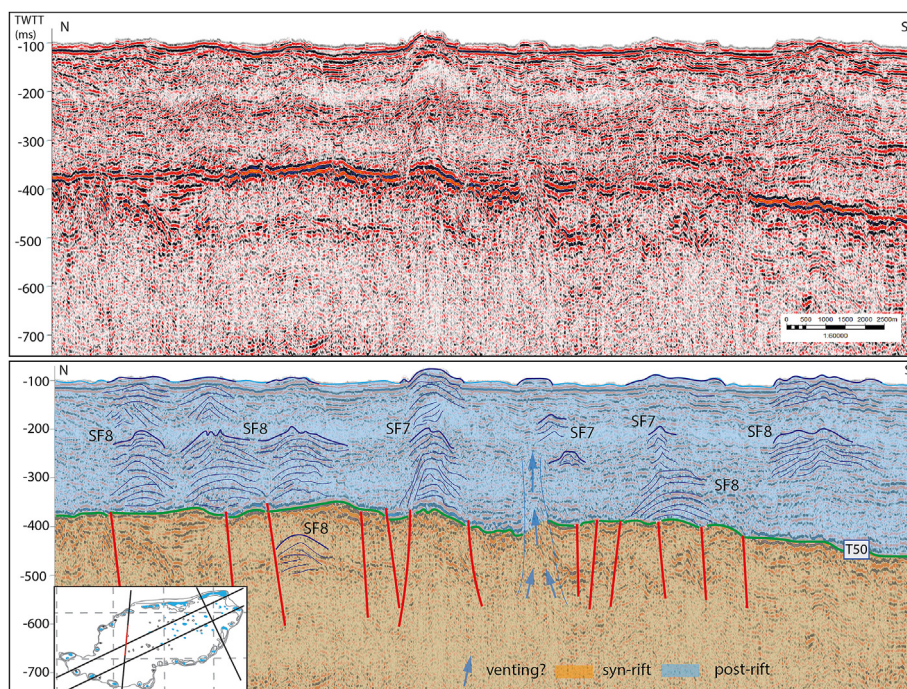


Fig. 8. Pinnacle and patch reefs dominated deposition in the lagoon during the post-rift phase.

reefs reveal pronounced differences in size and asymmetry consistent with the expected windward-leeward effect (Fig. 8). At the windward margin, reef mounds appear at continuous elevation and with less evidence for platform-derived sediment supply, reflecting continuous wave activity. At the leeward-margin, we observe more platform-derived sediment supply, leading to limited progradation at the expense of basin floor accumulation (Fig. 4).

Reef development in the lagoons started in the Middle Miocene. Both pinnacle and patch reefs are present. In the seismic reflection profiles, pinnacle reefs appear as spiky or conical packages bounded by strong reflectors that are partly highly attenuated (Table 1). Internally, the pinnacle reefs show relatively low reflection amplitudes, but some reveal evidence of layering. Interpretation of the internal character of pinnacle reefs becomes increasingly difficult as they decrease in size towards the lower limit of seismic resolution (Fig. 7A). Their internal reflectors are attenuated, but are displayed, layered and subparallel to sea bottom (Figs. 7 and 8, Table 1).

4.4. Seismic pipes and venting system

We also identify some evidence of fluid-flow (venting) features. These so-called chimneys or pipes appear as vertical zones of chaotic reflections, often associated with vertical zones of discontinuous reflectivity. Due to the lack of independent constraints, we use the well-known 'fluid-flow interpretation' system, which is now frequently used on 3D modern marine-seismic data (Ho et al., 2018; Hustoft et al., 2007), to identify potential fluid flow features in the four available seismic lines.

In our seismic profiles, pipes appear as vertical to sub vertical zones of highly discontinuous or disturbed reflections, or even as zones of complete loss of coherence (Fig. 9). Their appearance is often marked by seismic artefacts such as migration anomalies, scattering artefacts, lateral velocity anomalies and attenuation artefacts related to shallow diffractors. Up-doming of sub-surface parallel reflectors is observed, for example from -0.7 to about -0.2 s TWT in Fig. 9B. The up-doming is suspected to be a seismic pull-up artefact, because it diminishes with

depth and there is reason to expect a high acoustic velocity within a body composed of cemented sediments in the surface reef or mud-mound structure (Hovland et al., 2010; Hovland and Judd, 1988).

5. Discussion

A seismic stratigraphic scheme showing the distribution of distinct facies has been developed for the sedimentary succession of the Zhongsha atoll (Figs. 3 and 4, Table 1). The Zhongsha atoll likely shares a similar growth history with the Xisha platform, whose growth over a long period of time was controlled by subsidence rate, sea level fluctuations, carbonate production, terrigenous input, and ocean currents (Ma et al., 2011; Wu et al., 2014; Shao et al., 2017). The Zhongsha atoll is completely submerged under water. Zhongsha and Xisha are continental remnants that were not tectonically isolated from one another till the Early Miocene (Briais et al., 1993; Taylor and Hayes, 1980). Both XK-1 and XY-1 wells from Xisha resolved a thickness of more than 1200 m of carbonate. The Zhongsha atoll is situated on a more distal fault terrace to the east and may have experienced greater subsidence as a result of more crustal extension. Continuous subsidence allowed for the creation of accommodation space for the growth of an over 500 m thick marine carbonate succession. Tentative seismic stratigraphy, seismic stacking patterns, platform architecture, and depositional facies allow us to identify two major depositional phases: syn-rift and post-rift, for Zhongsha's evolution (Fig. 10).

5.1. Syn-rift phase (Units A, B, C) and post-rift phase (D, E, F)

Rifting of Zhongsha started in Paleogene times and accompanied a period of subaerial exposure during the late Eocene and Oligocene (Fig. 10A and B, C). In the southwest of Zhongsha, sediments accumulated in active grabens that experienced distinct periods of extension, as evidenced by thickness changes (Figs. 5 and 6). The space of accumulation of hundreds of meters of carbonate over the Zhongsha block during the Late Oligocene-Early Miocene (unit C) was mainly driven by its subsidence (Figs. 4 and 10). By comparison to the Xisha

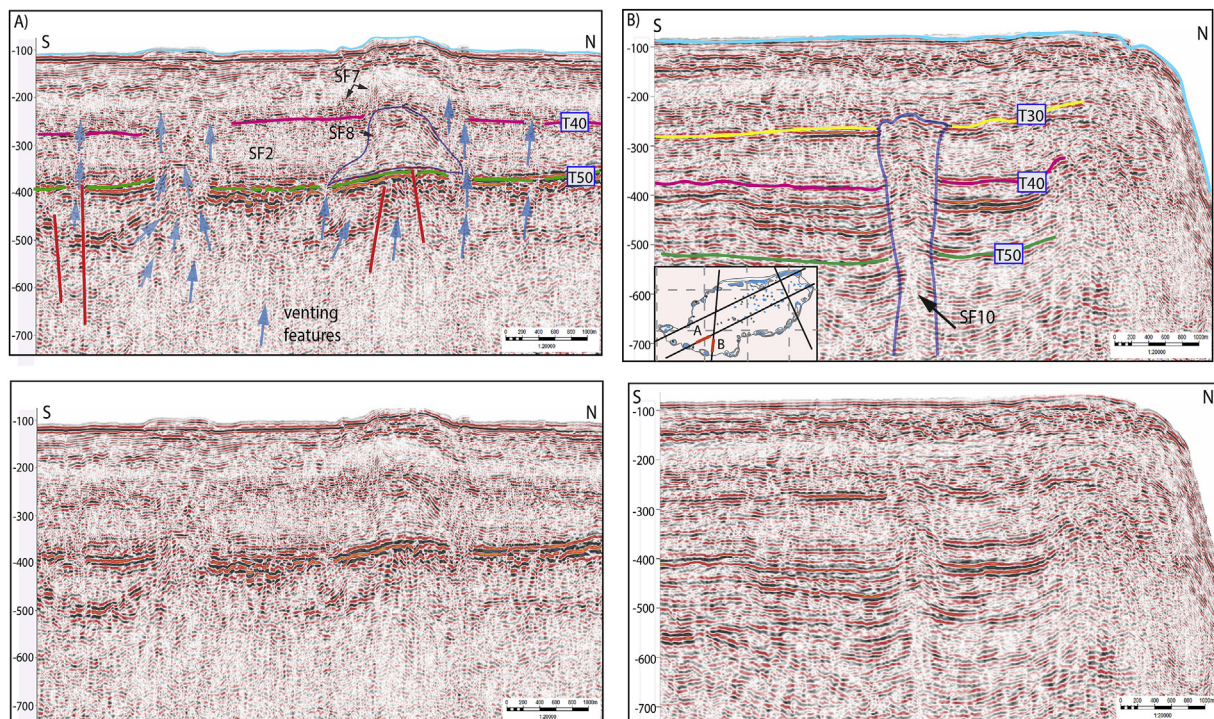


Fig. 9. Seismic chimneys or pipes. Reflection amplitudes within the pipe are generally highly variable, with localized amplitude anomalies distributed within or immediately adjacent to the pipe.

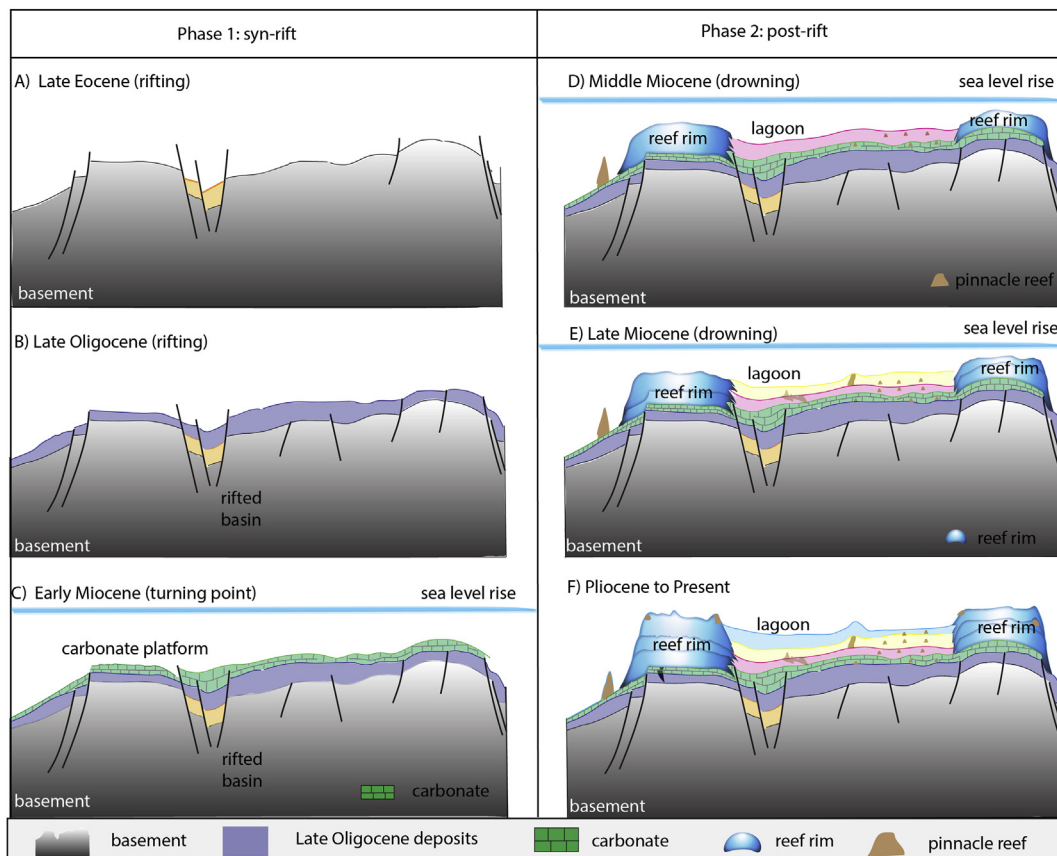


Fig. 10. Evolutionary model of the Zhongsha sedimentation history. Sedimentation was controlled by syn-rift tectonic subsidence and post-crustal thinning subsidence. The atoll started to form after the Middle Miocene.

Platform, it is likely that this subsidence accompanied ongoing rifting into Miocene times when carbonate platforms began to develop on individual footwall blocks in Zhongsha's Precambrian or Mesozoic metamorphic basement (Fig. 10). NE-SW trending fault planes dissecting the Zhongsha carbonate platform show that it may have suffered later fragmentation by tilting and vertical motion. Most of these faults accommodate a relatively small throw in the carbonate deposits (Figs. 4 and 5).

More than 200 m of northward-onlapping carbonate sediment in the northern part of the platform indicates the earlier onset of carbonate production there than in the south. As noted above, the Early Miocene carbonate platform may have initiated as reefs on tilted blocks. The platform aggraded and/or backstepped in response to an overall rise in relative sea level that was probably mainly driven by syn-rift subsidence during crustal extension (SF4) (Table 1). Relative thick carbonate sequences on the footwall blocks indicate that Zhongsha was subsiding fast, and corals on topographic highs had the highest chances of survival. The rapid subsidence might attributable to crustal thinning, as might be expected during rifting. The top of the carbonate platform (T50) shows denuded topography, possibly as a result of exposure and tilting during reactivation of the normal faults in the early Middle Miocene. The denudation could be related to glacio-eustatic drop in sea level, leading to extensive meteoric flushing of the shallow carbonate platform. Such events created marked unconformities in Miocene reefal sediments as revealed by seismic data (T50, and T40 surfaces, Fig. 4).

An atoll system initiated in the Middle Miocene and continued growing through Miocene till present time (Figs. 10 and 11). Rapid thermal subsidence was a key factor in atoll development, as has been shown elsewhere in the SCS (Hutchison et al., 2010; Wu et al., 2014; Shao et al., 2017). The rift processes at the transition from extension of continental lithosphere to the formation of oceanic crust is well studied

in the SCS (Clift and Lin, 2001; Su et al., 1989). This relatively young marginal basin is currently in a stadium which is characterized by still preserved differences in subsidence and thermal history resulting from rifting. The initial, complex and hardly quantifiable rift processes, however are long enough ago. The post-rift shallow water platform carbonates northern SCS indicate a delay in subsidence during rifting in the South China Sea (Franke et al., 2014). The first phase of rapid subsidence at Xisha occurred at 10.5–8.2 Ma, and a second after 5.5 Ma (Li et al., 2015). We propose that Zhongsha atoll was also affected by these drowning events in the Late Miocene and Early Pliocene, on the basis of episodic pinnacle reefs and patch reefs observed in the lagoons of units D, E, and F (Fig. 10).

Seismic facies and geometries reveal phases of platform aggradation, progradation and erosion that reflect the history of major relative sea-level fluctuations. The contrast between windward and leeward flanks of the platform seems to be more pronounced along the bank margin and uppermost slope (Fig. 4). The absence of well constraints makes precise correlation of the major seismic unit boundaries with eustatic curves rather difficult.

5.2. The major Middle Miocene turning point (T50)

The prominent high-amplitude single reflection marked as T50 (Middle Miocene) occurs throughout the dataset. This key horizon is characterized by a high contrast in acoustic impedance. It truncates underlying reflections, and the sedimentary sequence above onlaps onto it and marks an abrupt change in the seismic reflection patterns (Figs. 5 and 6). A prominent carbonate platform terminates at T50, and the upper part of the Miocene carbonate above T50 are characterized by smooth, concentric seismic reflections that form convex mounds, which indicate the onset of an atoll system in the Middle Miocene. Atoll

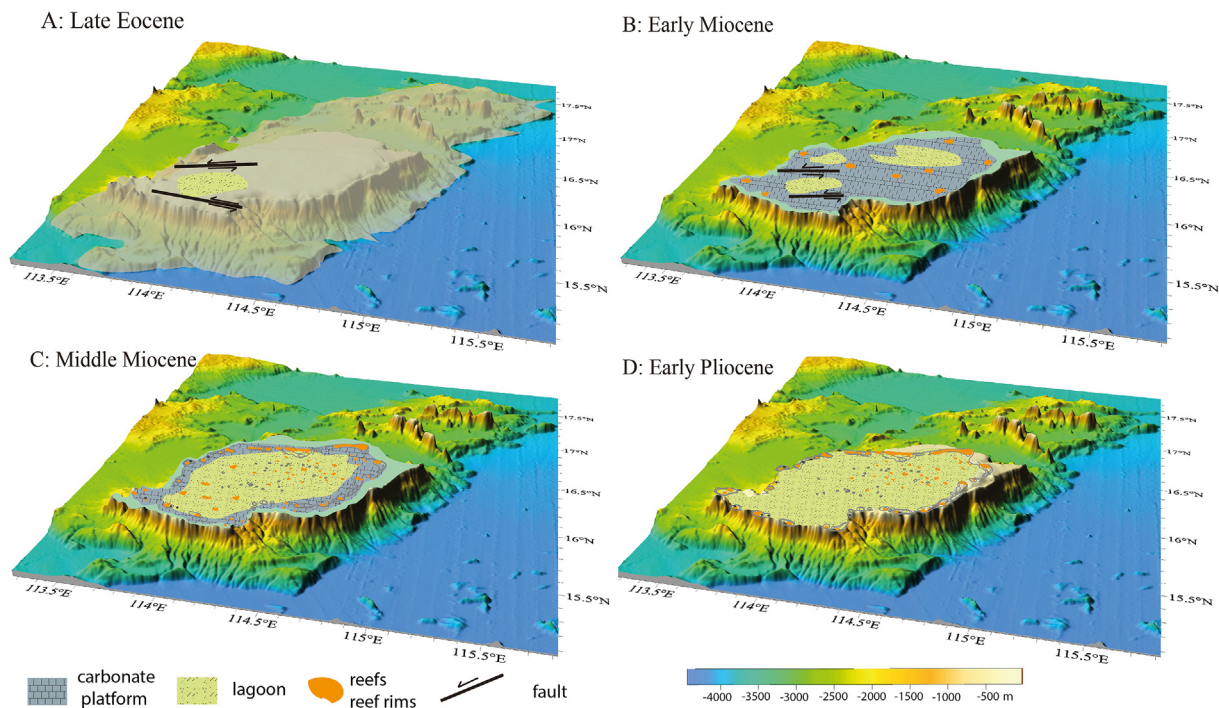


Fig. 11. Summary of lagoon and reef evolution during four different episodes. A: grabens generated by strike-slip and normal faults, no reefs; B: Carbonate platform developed over the entire Zhongsha atoll; C: Carbonate platform shrank, lagoon and reefs partly occupied Zhongsha; D: Lagoon and reefs dominated, carbonate platforms completely drowned.

formation may have resulted from a major Middle Miocene increase in accumulation rate, so that the lagoon could not be filled and an ‘empty bucket’ geometry formed, i.e. the platform underwent a partial drowning (Betzler et al., 2015). Drowning occurs where the rate of relative sea level rise exceeds a platform’s vertical accumulation rate for long enough that the platform descends beneath the euphotic zone, removing the photosynthetic basis for further growth (Schlager, 2005). Only those parts of the platform situated upon structural highs within Zhongsha survived, and those which kept pace with rising sea level formed reef rims. Both global (Miller et al., 2011) and local relative sea level curves, reconstructed using well data in of northern SCS, suggest a rapid sea level rise in the Early Miocene (15–16 Ma) (Fig. 3).

We suspect that this regional drowning event may also correspond to the Middle Miocene Climatic Optimum (MMCO), a period of relative global warmth at 17–15 Ma. Geological proxy records, including global stacks of $\delta^{18}\text{O}$ and $\delta^{13}\text{C}$ benthic foraminifers, indicate the MMCO featured above-present temperatures, relatively high atmospheric CO_2 , and a substantially reduced Antarctic Ice Sheet (Zachos et al., 2008; Huang et al., 2017). The MMCO led to an extension of the tropical belt and favored the wide distribution of coral communities. After the MMCO, renewed global cooling appears to have begun at ~ 14.2 Ma (Shevenell et al., 2004). The subsequent glacial expansion drove a 0.7 to 1.0 per mil increase in seawater and benthic foraminiferal $\delta^{18}\text{O}$ (Billups and Schrag, 2003) and a lowering of sea level by $\sim 40 \pm 15$ m (Miller et al., 2011). At Zhongsha, the Middle Miocene to present change in depositional style in the interior of the platform is seen as a result of the development of a broad, atoll-like platform, rimmed by reefs and having a relatively deep lagoon (Figs. 10 and 11).

5.3. Lagoon and reef evolution

The evolution of Zhongsha’s atoll and reefs was in three major phases: initial phase, growth phase, reef-dominated phase. Vertical accretion in the platform interior continued without a well-defined stratigraphic break (Figs. 10 and 11). Here, the most prominent depositional elements include lagoons (indicated by SF2), clinoforms

(SF3), reef rims (SF6), and pinnacle and patch reefs (SF7, 8), which composed the atoll system (Table 1). Further deepening caused local back-stepping of reef rims (SF4), and progradation of leeward margins into the lagoon (Fig. 4).

The very earliest lagoon was formed by subsidence against NW-SW and E-W trending faults from Late Eocene to Early Oligocene times, during the rifting process (Figs. 5 and 10). The lagoon was probably filled by shallow-water clastic sediments, inhibiting the development of reefs. During the post-Middle Miocene growth phase, the lagoon was sheltered from storms and wave action by reef rims. These rims were dissected by deep passages, allowing for strong currents to enter the atoll lagoon and the subsequent sediment reworking and redeposition, as well as for the growth of patch/pinnacal reefs (Ciarapica and Passeri, 1993) (Figs. 10 and 11). Most of the faults with NE-SW and E-W trend terminate slightly above or on top of the Middle Miocene strata.

During the lagoon and reef-dominant phase, a large atoll and abundant organic reefs initiated on positive relief, closely mimicking the underlying Early Miocene rift topography (Fig. 10B; C, D, Fig. 11C and D). These reefs continued growing vertically whilst most of the preexisting Early Miocene reefs and carbonate platform were drowned. The lagoon gradually filled in with a mixture of carbonate sediments produced there, and to a greater extent at the more productive reef rim (Fig. 6). Sedimentation resumed with the growth of reefal-slope wedges, which exhibit oblique clinoforms (SF3), which lap down on to the truncation surfaces and steepen basinwards (Fig. 6). The lagoon is sheltered in comparison to the outside of the atoll, and may host scattered knolls, and patch and pinnacle reefs, which are particularly abundant in the Miocene strata (Figs. 7, 8, 10). Seismic reflection profiles show that the Middle Miocene to present wedge-shaped lagoon deposits strongly truncate the underlying layer, which indicates sediment transport by gravity flow from atoll reefs and reef rims.

Favorable conditions in water depth, nutrient supply, and/or seabed morphology are likely to be the underlying controlling factors responsible for development of atoll reefs on Zhongsha. Zhongsha is located in the main field of the East Asian monsoons. North-easterly winds dominate the region in winter and south-westerly winds prevail

in summer (Clift et al., 2014). The monsoon plays a significant role in shaping the shallow-water topography under Zhongsha. Monsoon wind-driven currents and topographically-induced upwelling impinged on carbonate platforms beginning at about 13 Ma (Shao et al., 2017). Pre-existing topography is an important control on the facies geometries of the Zhongsha atoll by providing large-scale energy barriers that result in distinctive windward to leeward facies variability (Fig. 4). The extraordinary position and topography of the continental slopes, and the circulation of deep-sea currents create favorable conditions for forming coral reefs and promoting upwelling, which provide rich nutrients for reef-building organisms on the submarine platforms. The growth rate of the reef-building organisms and the accumulation of carbonate depend on winds, waves and currents (Wang and Li, 2009a, b).

Canyons were possibly formed by both slumping and erosion of turbidity currents, at times when the Zhongsha atoll was formed and T40 and T30 surfaces developed (Fig. 2) (Klaus and Taylor, 1991; Pratson et al., 1994). During submerged times, like today, they turn into submarine canyons, which may promote the development of upwelling currents and provide the hydrodynamic conditions favored by reef-building corals and other organisms. Downslope processes include turbidity currents and mass wasting which are strong enough as to deepen the canyons (Fig. 2).

5.4. Fluid flow and the linkage with reef growth

Our results document a number of seismic anomalies that resemble fluid-flow features on the Zhongsha atoll (Fig. 9). These features concentrate in areas of the Late Oligocene-Early Miocene platform and are also associated with pre-Miocene faults. The fluid-flow features could therefore be conduits for geothermally-heated pore waters or gas (Wang et al., 2018a, b). There appears to be no consistent pattern in the spacing of the hydrothermal vents relative to fault length, geometry or intersection locations as is commonly observed when faults act as fluid flow conduits. Given the complex distribution of faults (Figs. 3, 4 and 8), we suggest that interaction between all the aforementioned fault array properties locally influenced the fluid flow.

There are, however, carbonate buildups that feature numerous discontinuous hard-grounds (producing surfaces with high impedance contrasts which may blanked the underlying reflections), widespread liquid- and gas-filled compartments and pores at a variety of scales (producing, for example 'soft' and 'reverse' reflections). This diversity gives rise to numerous diffractions and areas of chaotic reflectivity, which may mislead the interpretation of the seismic profiles of such successions, particularly in the absence of a well control. Seismic artefacts (velocity anomalies, attenuation, transmission, and scattering) and the complexity of imaging the margins of a near-vertical geological feature whose width is often not much greater than the spatial resolution of the seismic data set combine to make the interpretation of details in the fluid flow structures extremely difficult. This task would have to await the availability of 3D seismic reflection data.

6. Conclusions

Subsidence at Zhongsha atoll (Macclesfield Bank) occurred in two major phases: a syn-rift phase and a post-rift phase. Reefs and an extensive lagoon developed during the post-rift phase, whose onset is marked by a turning point around the time of the formation of reflector T50. Large atolls formed, including organic reefs (pinnacle reefs, patch reefs) inside the lagoon, the reef rim initiated on positive relief, closely mimicking the underlying topography created by faults that were active during the Early Miocene. Three drowning events, occurring immediately after the formation of three regional reflectors T50 (Middle Miocene), T40 (Late Miocene), and T30 (Early Pliocene), are identified and are thought to tentatively imply three episodes of fast sea floor spreading in the study region. Pre-existing topography is an important control on facies geometries of the Zhongsha atoll by providing large-

scale energy barriers. The platform slopes extend from the atoll margins to the deep-sea basin and are cut by submarine canyons, which promote the development of upwelling currents and may provide the hydrodynamic conditions required for reef-building corals and other organisms to flourish. The monsoon may also play a significant role in shaping deep-water topography and the evolution of the atoll system. Our first documentation of the Neogene sedimentation history of this climatic sensitive region provide an important paleoenvironmental context for future scientific drilling to better constrain the Asia Monsoon.

CRedit authorship contribution statement

Xiaoxia Huang: Conceptualization, Data curation, Formal analysis, Funding acquisition, Investigation, Methodology, Project administration, Resources, Software, Supervision, Validation, Visualization, Writing - original draft, Writing - review & editing. **Christian Betzler:** Writing - review & editing. **Shiguo Wu:** Project administration, Resources. **Anne Bernhardt:** Writing - review & editing. **Graeme Eagles:** Writing - review & editing. **Xiaohui Han:** Project administration, Resources. **Martin Hovland:** Writing - review & editing.

Declaration of competing interest

The authors declare that they have no known competing financial interests or personal relationships that could have appeared to influence the work reported in this paper.

Acknowledgments

We thank the captain and crew of R/V NH503 for the seismic data acquisition. The finance supports were from Pioneer Hundred Talents Program (Y910091001), China; the National Science Foundation of China (41976233), and the National Science Foundation of China (No. U1701245). Schlumberger is acknowledged for the donation of the Petrel (*) license.

Appendix A. Supplementary data

Supplementary data to this article can be found online at <https://doi.org/10.1016/j.marpetgeo.2020.104349>.

References

- Li, C.F., Li, J.B., Ding, W.W., Franke, D., Yao, Y.J., Shi, H.S., Pang, X., Cao, Y., Lin, J., Kulhanek, D.K., Williams, T., Bao, R., Briais, A., Brown, E.A., Chen, Y.F., Clift, P.D., Colwell, F.S., Dadd, K.A., Almeida, I.H., Huang, X.L., Hyun, S., Jiang, T., Koppers, A.A.P., Li, W.Y., Liu, C.L., Liu, Q.S., Liu, Z.F., Nagai, R.H., Alampay, A.P., Su, X., Sun, Z., Tejada, M.L.G., Trinh, H.S., Yeh, Y.C., Zhang, C.L., Zhang, F., Zhang, G.L., Zhao, X.X., 2015. Seismic stratigraphy of the central South China Sea basin and implications for neotectonics. *J. Geophys. Res. (Solid Earth)* 120, 1377–1399. <https://doi.org/10.1002/2014JB011686>.
- Barkhausen, U., Engels, M., Franke, D., Ladage, S., Pubellier, M., 2014. Evolution of the South China Sea: revised ages for breakup and seafloor spreading. *Mar. Petrol. Geol.* 58, 599–611.
- Betzler, C., Hübscher, C., Lindhorst, S., Reijmer, J.J., Römer, M., Droxler, A.W., Lüdmann, T., 2009. Monsoon-induced partial carbonate platform drowning (Maldives, Indian Ocean). *Geology* 37 (10), 867–870.
- Betzler, C., Fürstenau, J., Lüdmann, T., Hübscher, C., Lindhorst, S., Paul, A., Droxler, A.W., 2013. Sea-level and ocean-current control on carbonate-platform growth, Maldives, Indian Ocean. *Basin Res.* 25 (2), 172–196.
- Betzler, Christian, Sebastian, Lindhorst, Lüdmann, Thomas, Weiss, Weiss, Wunsch, Marco, Carlos Braga, Juan, 2015. The leaking bucket of a Maldives atoll: implications for the understanding of carbonate platform drowning. *Mar. Geol.* 366, 16–33.
- Billups, K., Schrag, D.P., 2003. Application of benthic foraminiferal Mg/Ca ratios to questions of Cenozoic climate change. *Earth Planet Sci. Lett.* 209, 1–2 181–195.
- Briais, A., Patriat, P., Tapponnier, P., 1993. Updated interpretation of magnetic anomalies and seafloor spreading stages in the South China Sea: implications for the Tertiary tectonics of Southeast Asia. *J. Geophys. Res.: Solid Earth* 98 (B4), 6299–6328.
- Burger, J., Gochfeld, M., 2000. Metal levels in feathers of 12 species of seabirds from Midway Atoll in the northern Pacific Ocean. *Sci. Total Environ.* 257 (1), 37–52.
- Ciarapica, Passeri, L., 1993. An overview of the Maldivian coral reefs in Felidu and north

- Male' Atoll (Indian Ocean): platform drowning by ecological crisis. *Facies* 28, 33–65.
- Clift, P., Lin, J., 2001. Preferential mantle lithospheric extension under the South China margin. *Mar. Petrol. Geol.* 18 (8), 929–945.
- Clift, P.D., Wan, S., Blusztajn, J., 2014. Reconstructing chemical weathering, physical erosion and monsoon intensity since 25 Ma in the northern South China Sea: a review of competing proxies. *Earth Sci. Rev.* 130, 86–102.
- Franke, D., Savva, D., Pubellier, M., Steuer, S., Mouly, B., Auxietre, J.L., Chamot-Rooke, N., 2014. The final rifting evolution in the South China Sea. *Mar. Petrol. Geol.* 58, 704–720.
- Fyhn, M.B., Boldreel, L.O., Nielsen, L.H., Giang, T.C., Nga, L.H., Hong, N.T., Abatzis, I., 2013. Carbonate platform growth and demise offshore Central Vietnam: Effects of Early Miocene transgression and subsequent onshore uplift. *J. Asian Earth Sci.* 76, 152–168.
- Fyhn, M.B., Boldreel, L.O., Nielsen, L.H., 2009. Tectonic and climatic control on growth and demise of the Phan Rang Carbonate Platform offshore south Vietnam. *Basin Res.* 21 (2), 225–251.
- Gao, J.W., Wu, S.G., McIntosh, K., Mi, L.J., Liu, Z., Spence, G., 2016. Crustal structure and extension mode in the northwestern margin of the South China Sea. *Geochem. Geophys. Geosyst.* 17, 2143–2167.
- Ha, K., Seo, Y., Lee, J., et al., 2018. Linkages between the South and East Asian summer monsoons: a review and revisit. *Clim. Dynam.* 51, 4207–4227. <https://doi.org/10.1007/s00382-017-3773-z>.
- Haq, B.U., Hardenbol, J., Vail, P.R., 1987. Chronology of Fluctuating Sea levels since the Triassic. *Science* 235, 1156–1167. <https://doi.org/10.1126/science.235.4793.1156>.
- Ho, S., Imbert, P., Hovland, M., Wetzel, A., Blouet, J.P., Carruthers, D., 2018. Downslope shifting pockmarks: interplay between hydrocarbon leakage, sedimentations, currents and slope's topography. *Int. J. Earth Sci.* 107 (8), 2907–2929.
- Hovland, M., Judd, A.G., 1988. Seabed Pockmarks and Seepages: Impact on Geology, Biology and The Marine Environment. Graham & Trotman, Ltd, London, pp. 293.
- Hovland, M., Heggland, R., De Vries, M.H., Tjeltnes, T.I., 2010. Unit-pockmarks and their potential significance for predicting fluid flow. *Mar. Petrol. Geol.* 27 (6), 1190–1199.
- Huang, X., Stürz, M., Gohl, K., Knorr, G., Lohmann, G., 2017. Impact of Weddell Sea shelf progradation on Antarctic bottom water formation during the Miocene. *Paleoceanography* 32 (3), 304–317.
- Huang, H.B., Qiu, X.L., Pichot, T., Klingelhoefer, F., Zhao, M.H., Wang, P., Hao, T.Y., 2019. Seismic structure of the northwestern margin of the South China Sea: implication for asymmetric continental extension. *Geophys. J. Int.* 218 (2), 1246–1261.
- Hustoft, S., Mienert, BünzS., Nouze, H., 2007. High-resolution 3D-seismic data indicate focussed fluid migration pathways above polygonal fault systems of the mid-Norwegian margin. *Mar. Geol.* 245, 89–106.
- Hutchison, C.S., 2010. The north-west Borneo trough. *Mar. Geol.* 271, 32–43.
- Jorry, S.J., Bièvre, G., 2011. Integration of sedimentology and ground-penetrating radar for high-resolution imaging of a carbonate platform. *Sedimentology* 58 (6), 1370–1390.
- Klaus, A., Taylor, B., 1991. Submarine canyon development in the Izu-Bonin forearc: a SeaMARC II and seismic survey of Aoga Shima canyon. *Mar. Geophys. Res.* 13 (2), 131–152. <https://doi.org/10.1007/BF00286285>.
- Li, C.F., Li, J.B., Ding, W.W., Franke, D., Yao, Y.J., Shi, H.S., Pang, X., et al., 2015. Seismic stratigraphy of the central South China Sea basin and implications for neotectonics. *J. Geophys. Res. Solid Earth* 120, 1–23.
- Li, Q., Wang, P., Zhao, Q., Shao, L., Zhong, G., Tian, J., Su, X., 2006. A 33 Ma lithostratigraphic record of tectonic and paleoceanographic evolution of the South China Sea. *Marine Geology* 230 (3–4), 217–235.
- Lukaski, J., Simo, J.A., Schlager, W., 2008. Controls on Carbonate Platform and Reef Development, vol. 89 SEPM Special Publication.
- Martin, J.M., Braga, J.C., Betzler, C., Brachert, T., 1996. Sedimentary model and high-frequency cyclicity in a Mediterranean, shallow-shelf, temperate-carbonate environment (uppermost Miocene, Agua Amarga Basin, Southern Spain). *Sedimentology* 43 (2), 263–277.
- Ma, Y., Shiguo, W., Fuliang, L., Dongdong, D., Qiliang, S., Yintao, L., Mingfeng, G., 2011. Seismic characteristics and development of the Xisha carbonate platforms, northern margin of the South China Sea. *J. Asian Earth Sci.* 40 (3), 770–783.
- Miller, K.G., Moutaers, G.S., Wright, J.D., Brown, J.V., 2011. A 180-million-year record of sea level and ice volume variations from continental margin and deep-sea isotopic records. *Oceanography* 24 (2), 40–53.
- Nissen, S.S., Hayes, D.E., Bochu, Y., Weijun, Z., Yongqin, C., Xiaopin, N., 1995. Gravity, heat flow, and seismic constraints on the processes of crustal extension: northern margin of the South China Sea. *J. Geophys. Res.* 100, 447–483.
- Pratson, L.F., Ryan, W.B., Mountain, G.S., Twichell, D.C., 1994. Submarine canyon initiation by downslope-eroding sediment flows: evidence in late Cenozoic strata on the New Jersey continental slope. *Geol. Soc. Am. Bull.* 106 (3), 395–412.
- Qiu, X.L., Zhao, M.H., Ye, C.M., Wang, T.K., Wang, P., Zhang, Y.X., Lee, C.S., 2004. Ocean bottom seismometer and onshore-offshore seismic experiment in northeastern South China Sea. *Geotectonica et Metallogenia* 28 (1), 28–35.
- Qiu, Y., Wang, Y.M., 2001. Reefs and paleostructure and paleoenvironment in the south China sea. *Mar. Geol. Quat. Geol.* 21 (1), 65–74.
- Schlager, W., 1999. Scaling of sedimentation rates and drowning of reefs and carbonate platforms. *Geology* 27 (2), 183–186.
- Schlager, W., 2005. Carbonate sedimentology and sequence stratigraphy. *SEPM Concepts Sedimentol. Paleontol.* 8, 209.
- Shevenell, A.E., Kennett, J.P., Lea, D.W., 2004. Middle Miocene southern ocean cooling and Antarctic cryosphere expansion. *Science* 305 (5691), 1766–1770. <https://doi.org/10.1126/science.1100061>.
- Su, D., White, N., McKenzie, D., 1989. Extension and subsidence of the pearl river mouth basin, northern South China sea. *Basin Res.* 2, 205–222.
- Sun, Z., Zhong, Z.H., Keep, M., Zhou, D., Cai, D.S., Li, X.S., Wu, S.M., 2009. 3D analogue modeling of the South China Sea: a discussion on breakup pattern. *J. Asian Earth Sci.* 34 (4), 544–556.
- Shao, L., Li, Q., Zhu, W., Zhang, D., Qiao, P., Liu, X., Dong, X., 2017. Neogene carbonate platform development in the NW South China Sea: Litho-, bio- and chemo-stratigraphic evidence. *Mar. Geol.* 385, 233–243.
- Taylor, B., Hayes, D.E., 1980. The tectonic evolution of the South China Basin. *Tectonic Geol. Evol. Southeast Asian Seas and Islands* 23, 89–104.
- Taylor, B., Hayes, D.E., 1983. Origin and history of the south China sea basin. *Tectonic Geol. Evol. Southeast Asian Seas and Islands: Part 2*, 23–56.
- Wang, P.X., Li, Q.Y., 2009a. The South China Sea: Paleoceanography and Sedimentology. Springer, the Netherlands.
- Wang, P., Li, Q. (Eds.), 2009. The South China Sea — Paleoceanography and Sedimentology. Springer, Dordrecht.
- Wang, P., Li, Q., Tian, J., Jian, Z., Liu, C., Li, L., Ma, W., 2014. Long-term cycles in the carbon reservoir of the Quaternary ocean: a perspective from the South China Sea. *Nat. Sci. Rev.* 1, 119–143. <https://doi.org/10.1093/nsr/nwt028>.
- Wang, Z., F C, Y. C., Shao, L., 2015. Carbonate platform development and sea-level variations of Xisha Islands: based on BIT index of Well Xike-1. *Earth Sci. J. China Univ. Geosci.* 44 (5), 900–908 (in Chinese).
- Wang, J., Wu, S., Yao, Y., 2018a. Quantifying gas hydrate from microbial methane in the South China Sea. *J. Asian Earth Sci.* 168, 48–56.
- Wang, J., Wu, S., Kong, X., Ma, B., Li, W., Wang, D., Chen, W., 2018b. Subsurface fluid flow at an active cold seep area in the Qiongdongnan Basin, northern South China Sea. *J. Asian Earth Sci.* 168, 17–26.
- Wilson, M.E., 2008. Global and regional influences on equatorial shallow-marine carbonates during the Cenozoic. *Palaeogeogr. Palaeoclimatol. Palaeoecol.* 265 (3–4), 262–274.
- Wu, S., Yang, Z., Wang, D., Lü, F., Lüdmann, T., Fulthorpe, C., Wang, B., 2014. Architecture, development and geological control of the Xisha carbonate platforms, northwestern South China Sea. *Mar. Geol.* 350, 71–83.
- Wu, S., Zhang, X., Yang, Z., Wu, T., Gao, J., Wang, D., 2016. Spatial and temporal evolution of Cenozoic carbonate platforms on the continental margins of the South China Sea: response to opening of the ocean basin. *Interpretation* 4 (3), SP1–SP19.
- Xiu, C., Luo, W., Yang, H., Zhai, S., Liu, X., Cao, J., Liu, X., Chen, H., Zhang, A., 2015. Geochemical characteristics of reef carbonate rocks in well Xike-1 of Shidao Island, Xisha area. *Earth Sci. J. China Univ. Geosci.* 40, 645–652 (in Chinese with English abstract).
- Yan, Q., Shi, X., Castillo, P.R., 2014. The late Mesozoic–Cenozoic tectonic evolution of the South China Sea: a petrologic perspective. *J. Asian Earth Sci.* 85, 178–201.
- Zachos, J.C., Dickens, G.R., Zeebe, R.E., 2008. An early Cenozoic perspective on greenhouse warming and carbon-cycle dynamics. *Nature* 451 (7176), 279–283.
- Zampetti, V., Schlager, W., van Konijnenburg, J.H., Everts, A.J., 2004. Architecture and growth history of a Miocene carbonate platform from 3D seismic reflection data; Luconia province, offshore Sarawak, Malaysia. *Mar. Petrol. Geol.* 21 (5), 517–534.
- Zampetti, V., Sattler, U., Braaksma, H., 2005. Well log and seismic character of Lihua 11-1 Field, South China Sea; relationship between diagenesis and seismic reflections. *Sediment. Geol.* 175 (1–4), 217–236.
- Zhang, G.L., Luo, Q., Zhao, J., Jackson, M.G., Guo, L.S., 2018. Geochemical nature of sub-ridge mantle and opening dynamics of the South China Sea. *Earth Planet Sci. Lett.* 489, 145–155.
- Zhu, Y., Liu, X., Ma, R., Luo, W., Wang, X., Xu, S., 2016. Early Miocene to quaternary calcareous nannofossils from the biogenetic reef complexes and their significance of well XK1, Xisha islands, south China sea. *Acta Palaeontol. Sin.* 55, 385–392 (in Chinese with English abstract).